EXPERIMENTAL TECHNIQUES WITH HIGHLY STABLE CLOCKS

ROBERT F. C. VESSOT
Smithsonian Astrophysical Observatory, Cambridge, Massachusetts, 02138, USA

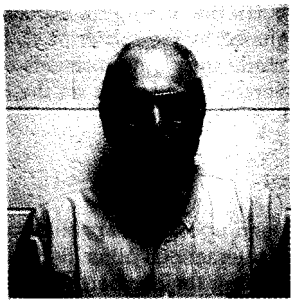

ABSTRACT

Modern metrology depends increasingly on the accuracy and frequency stability of atomic clocks. While *accuracy* of measurement with respect to the defined second of time is important for many aspects of metrology, the precision of experimental measurements depends very strongly upon the *stability* of the clock during the data-taking process. Today's atomic hydrogen masers produce signals with fractional frequency stability better than 1×10^{-15} over intervals of 10^3 to 10^5 seconds Operation of a cryogenically cooled H-Maser has been demonstrated and the prospects for getting frequency stability better than 1×10^{-16} appear to be realistic. Multi-link microwave systems to cope with the Doppler effect of spacecraft motion and of signal propagation through the earth's troposphere and ionosphere are described, including methods using time-correlation to cancel localized disturbances in very long signal paths. Applications of such high-stability oscillators (or clocks) to experiments performed in space are described and estimates of the precision of these experiments are made in terms of clock performance. Analyses of proposed tests of relativistic gravitation, of operation of a very long baseline interferometry (VLBI) system operated in space, and of a possible measurement of the quadrupole moment of the sun's mass distribution are discussed. A proposed space borne four-stationVLBI system is described that could compare, with a precision of 3×10^{-15} rad/sec, the rotation of a local inertial frame based on the velocity of light with the inertial frame defined by distant radio stars. This system could provide information on the behavior of missing matter.

1. Introduction

Time and frequency are the present basis of metrology. In 1967 the unit of time was defined as 9,192,631,770 cycles of the hyperfine separation (HFS) of Cesium 133; in 1983, the meter was defined as the distance light travels in 1/299,792,458 of a second. Today, the accuracy in our manifestation of the ^{133}Cs HFS frequency is the basis for accurate measurement of time and length.

We must be careful to distinguish between accuracy and stability. Accuracy is the quality that relates a frequency to an absolute number, for example, the theoretical definition of the hyperfine separation of Cesium 133. Frequency stability is a measure of how the frequency varies with time. The most currently used measure of frequency stability is the Allan deviation, $\sigma_y(t)$, the one-sigma expectation of the fractional frequency difference, $\Delta f/f$, (designated by the subscript y), between time-adjacent frequency measurements, each made over time intervals of duration, τ. The functional relationship of $\sigma_y(t)$ versus (τ) depends on the Fourier spectrum of of the phase or frequency variations.[1)]

1.1 Methodology of atomic clocks

Modern atomic clocks depend upon the capability of keeping an ensemble of atoms (or ions) isolated from all interactions other than the stimulating radiation required to produce transitions among their hyperfine levels. According to Heisenberg's uncertainty principle, the linewidth of these transitions will be equal to the inverse of the time they spend in isolation. Many techniques are available to provide a degree of such isolation. The earliest and traditional method is use of atomic beams where the duration of isolation is the flight time through the interaction region where signals are applied to make hyperfine transitions.

Confinement techniques with vessels specially coated to reduce spurious collisional effects with their interior walls are used for localizing ensembles of Hydrogen in H-Masers and for use of alkali atoms in experimental devices. Another method for low interactive confinement is with cells containing buffer gases that have little collisional effect with the active vapor atoms.

More recently, very long interaction times have been made possible by trapping ions using radio frequency (Paul) traps and magnetic (Penning) traps. The advent of modern laser techniques has opened up a whole new world of optical methods for pumping atoms and ions into the desired hyperfine sublevels and for detecting the hyperfine transitions with extremely high frequency resolution. The Zacharias cesium fountain conceived in the 1960s has been successfully revived using such optical techniques for manipulating atoms and controlling their movements. Papers elsewhere in this book by C, Salomon, K. Gibble and J. Prestage describe these new frequency discriminators.

It is important to recognize the difference between passive systems that provide extremely high levels of frequency discrimination and actively oscillating systems frequency that actually produce signals. To operate as frequency standards, frequency discriminators require highly stable controllable oscillators in conjunction with various modulating techniques to lock the the oscillator frequency to the center of the atomic or ionic line of the discriminator. The phase fluctuations of these oscillators

must be small over the interval required for interrogating the atom. As the storage time is made longer in the quest for higher frequency resolution, ever greater demands are made on the stability of the active oscillator.

1.2 The Atomic Hydrogen Maser

The atomic hydrogen Maser (H-maser) is the only active atomic oscillator in common use today. It is unique in having high frequency stability over intervals from 1 sec. to about 1 day; however, owing to the variability of the wall collision frequency shift, its accuracy capability is not suitable for use as a primary frequency standard. The stability of the H-maser can be described in terms of its physical parameters.

The fundamental limitation of the stability of the maser is described by

$$\sigma_y(\tau) = \frac{1}{Q_l}\left[\frac{kT}{2P\tau}\right]^{1/2} \qquad (1)$$

Here k is Boltzmann's constant, T is the physical temperature of the maser, $Q_l = \frac{\omega}{2\gamma_{2T}}$ is the oscillating line Q, $\omega = 2\pi f$ is the angular frequency of oscillation, and $\gamma_{2T} = \gamma_b + \gamma_{se} + \gamma_w + \gamma_m$ is the total transverse (phase loss) relaxation rate comprising the effects of loss of atoms in the bulb, γ_b ; spin-exchange collisions, γ_{se}; wall collision, γ_w; and magnetic inhomogeneity, γ_m.

Two distinctly different types of instability processes are dominant in the output signal of the H-maser: additive *white phase* noise associated with thermal noise, kT, per unit bandwidth that accompanies the signal, and the *white frequency* noise associated with the thermal noise, kT, within the line width of the oscillating atoms as given in equation 1. The effects of temperature are evident here and the benefits of operating at low temperatures will be apparent in the following discussion.

Under conditions of operation at optimum flux[2], (when $\gamma_{se} = \gamma_b + \gamma_w$)) the Allan deviation of the added *white phase noise* is:

$$\sigma_a(\tau) = \left[\frac{k\,[T_n + T]\,2\pi\,B\,\sigma v\,Q_{ext}\,I_{tot}}{h\,\omega^3\,V_b\,Q_{lo}\,I}\right]^{1/2}\frac{\tau^{-1}}{\gamma_b} \qquad (2)$$

Under the same conditions, the Allan deviation of the added *white frequency noise* is:

$$\sigma_f(\tau) = \left[\frac{16\pi kT\sigma_{se}\,v\,I_{tot}}{h\,\omega^3\,V_b\,I}\right] \qquad (3)$$

Here T_n is the noise temperature of the signal processing system, h is Planck's constant, $\sigma_{se}\,v$ is the spin-exchange cross section times the average velocity of the atoms, V_b is the volume of the atomic storage volume and $\tau_b = 1/\gamma_b$ is its storage time constant, B is the noise bandwidth of the measuring system, Q_{lo} is the loaded quality factor of the resonator, and Q_{ext} is the Q associated with the power delivered to circuits external to the cavity. I_{tot} /I is the ratio of the number of atoms in the desired F=1, m_F =0 state to the total atoms entering the storage bulb.

The dependence on temperature is clear in both these equations. We can expect considerable improvement by reducing the physical temperature, given that we can find ways to store the atoms without excessive perturbation.[3]. By operating the H-Maser at temperatures near 0.5 K with storage volume coatings of superfluid ^4H_e, very promising results have been obtained[4]. One important aspect of operation at these temperatures is that the combination of average velocity and cross section, sv, is reduced by a factor of 2000 times. This factor, combined with the temperature reduction factor $(300/0.5)^{1/2}$, shows the frequency stability, $\sigma_y(t)$, can be improved by a by a factor of about 350 times. Figure 1 shows the expected improvement in frequency stability of the cryomaser over that of conventional H-masers.

2. The effects of oscillator instability on measurements of distance and of range-rate using Doppler data.

Figure 2 shows $\sigma(\tau)$ versus t plots for atomic hydrogen masers[5], stored ion devices[6], and for the binary pulsar[7]. This figure also includes the Allan deviation of disturbances caused by the earth's troposphere and ionosphere on signals traversing vertically. In the following discussions of experimental techniques, the H maser performance data in Figure 2 will be used as a basis for numerical examples as well as for illustrations of methods to cancel propagation and Doppler effects between widely separated clocks.

Oscillator performance given by $\sigma_y(t)$ can provide statistical estimates of the limits imposed by clock performance on the precision of measurements.

An estimate of the time dispersion of a clock or oscillator for a future time interval, τ, can be obtained from the relation

$$\sigma_{\Delta\tau}(\tau) \sim \tau\, \sigma_y(\tau) \tag{4}$$

We can obtain an estimate of range dispersion from time dispersion given in Equation 4, For distance measurements made from the one-way propagation of light by writing

$$\sigma_{\Delta r}(\tau) = c\, \tau\, \sigma_y(\tau) \tag{5}$$

where c is the velocity of light.

Range rate measurements are made from the Doppler frequency shift, Δf, of signals from an oscillator transmitting at a frequency, f, moving with velocity v_r relative to the receiver:

$$\frac{\Delta f}{f} = \pm \frac{v_r}{c} \tag{6}$$

The contribution of the oscillator to the imprecision of determining range rate, v_r, during measurement intervals, τ, is given by

$$\sigma_{vr}(\tau) = c\, \sigma_y(\tau) \qquad (y = \Delta f/f) \tag{7}$$

Figure 3 is a nomograph of range-rate error and range distance error based on the H-maser data in Figure 2. On the left hand axes are scales for $\sigma_y(t)$ and the

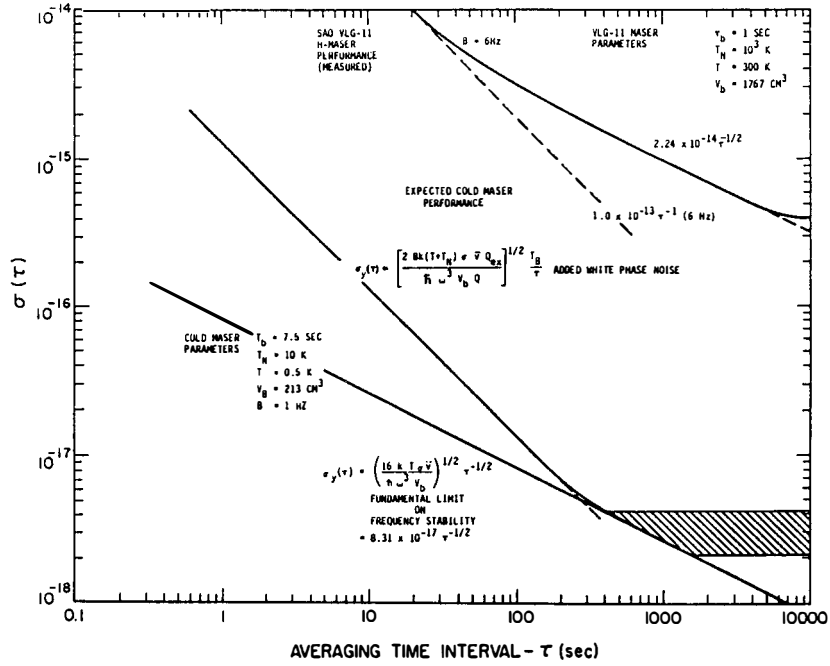

gure 1 Predicted cryo-maser performance

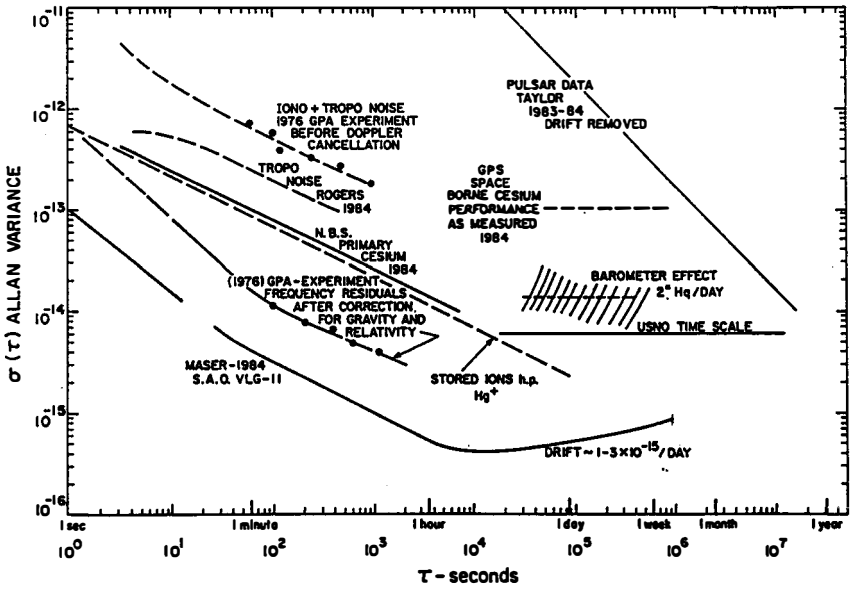

Figure 2 Frequency stability of oscillators and propagation effects

Figure 3

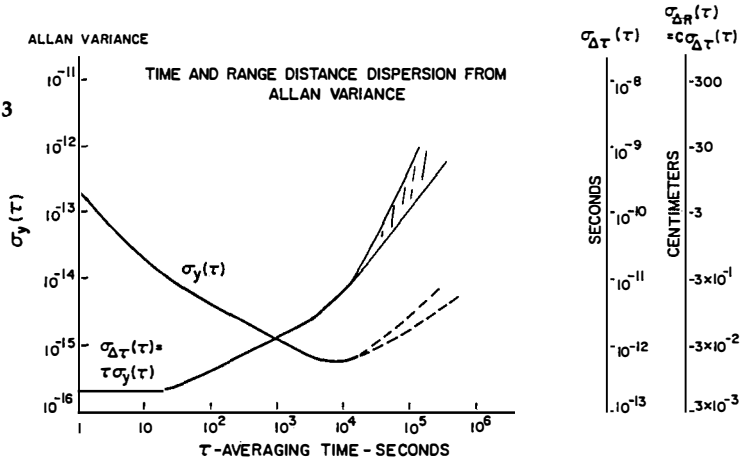

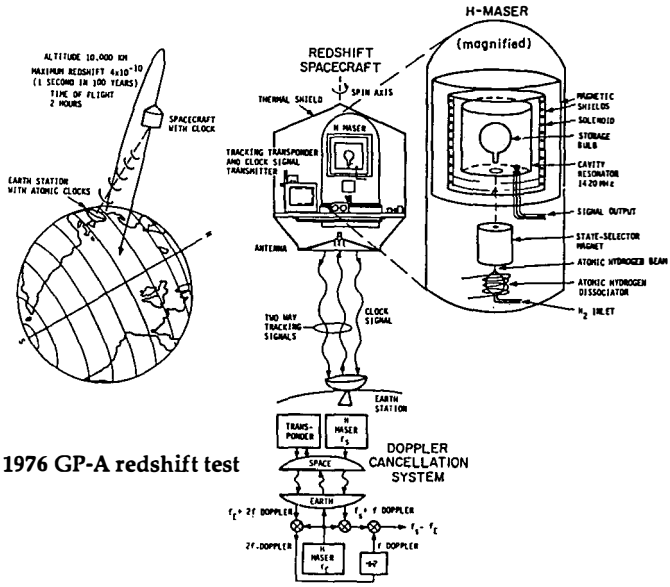

Figure 4 The 1976 GP-A redshift test

corresponding one-way Doppler frequency range-rate measurement error, $\sigma_{v_T}(t)$. On the right hand axes are the scales for time dispersion, $\sigma_{\Delta\tau}(t)$, and the corresponding one-way range measurement error.

2.1 Cancelling First-Order Doppler , Signal Propagation Effects and Removal of Ionospheric Doppler Shifts

The cartoon in Figure 4 schematically describes the 1976 SAO-NASA Gravity Probe A (GP-A) test of the gravitational redshift, and the phase-coherent analog system that was used to cancel the effects of first-order Doppler and signal propagation anomalies between the earth and space H-Maser clocks. By measuring the Doppler effects in a *separate* two-way system and subtracting one-half the number of two-way cycles from the phase of the received signal in the one-way microwave link connecting the space vehicle clock to the earth station, the propagation effects were *systematically* removed.

A closer look at the Doppler cancelling system in Figure 4 is given in Figure 5. The phase coherence throughout the system was provided by ratio frequency synthesizers. Because of the 189 MHz difference in the uplink and downlink frequencies in the S-band (2 GHz) transponder, variations in the ionospheric electron content in the signal path would have caused serious time-variations in phase delay.

The total Doppler frequency shift, f_D, due to the signal path, including the refractive indices of the propagation medium, is given by

$$f_D = \frac{1}{fc}\frac{d}{dt}\int_P n(t)ds \qquad (8)$$

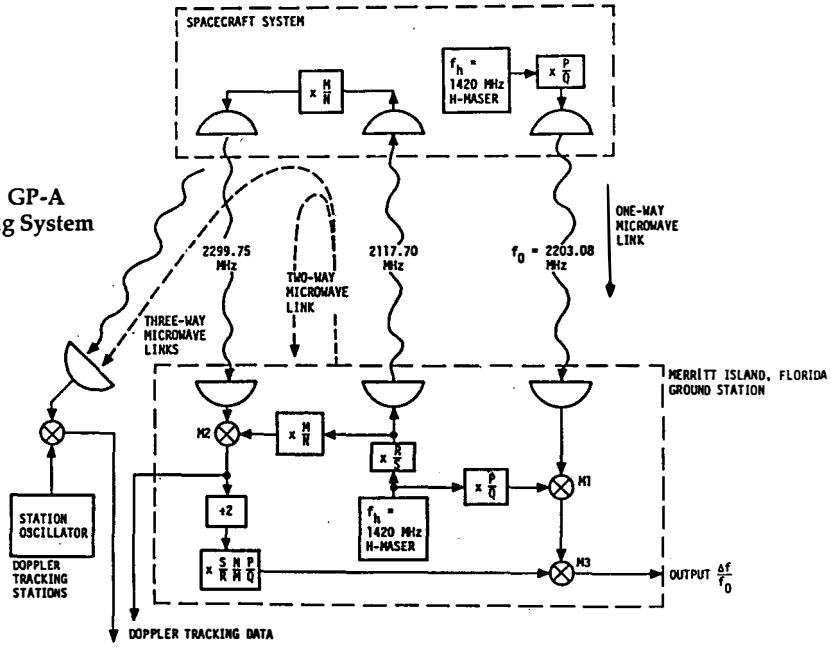

Figure 5 The 1976 GP-A Doppler Cancelling System

where $n(t) = n_A(t) + n_I(t)$ is the sum of the time-varying refractive indices of the atmosphere and the ionosphere respectively. The refractive index of the atmosphere, at the frequencies shown in Figure 5, has no significant frequency dependence and has no effect on the 3-link Doppler cancelation system when the propagation time is short compared to the measurement interval.

However, propagation through the time-varying ionosphere can cause large frequency variations in a received signal. In the 1976 test these shifts were estimated to be several parts in 10^{-10} and would have completely overwhelmed the data from the combined redshift and second-order Doppler effect.

Frequency shifts caused by variations in ionospheric electron density cause variations in the ionospheric refractive index as follows [8]

$$n_I = [1 - f_n^2/f^2(1-f_m/f)]^{1/2} \qquad (9)$$

where $f_m = m_o H e/2pm = 2.8$ MHz/Oersted, is the effect of the electron's magnetic interaction (which for S-band signals near earth is small, and in our case could be neglected). The quantity $f_n^2 = \rho e^2/(2\pi)^2 e_o m$, is the square of the electron plasma frequency. Here ρ is the electron density, e and m are the electron's charge and mass, and e_o is the permittivity of free space.

The frequency shift owing to the change in the amount of ionization in the propagation path f_{DI}, is given by including the expression (9) in equation (8) and expanding, neglecting the magnetic term.

$$f_{DI} = \frac{1}{f c}\frac{d}{dt}\int_p \left(1 - \frac{\rho e^2}{8\pi^2 \varepsilon_o m}\right) ds$$

$$= -\frac{e^2}{8\pi f c \varepsilon_o m}\frac{d}{dt}\int_p \rho(t)\, ds \qquad (10)$$

Here p is the propagation path over which the integral is taken. The integral represents the columnar electron density in the path. When we follow the ionospheric Doppler frequency shifts through the two transponder links and the clock downlink, we find that the ionosphere contributes a frequency error at the output from mixer M3 of Figure 5 in the amount

$$|f_{I\,error}| = \frac{e^2}{8\pi f c \varepsilon_o m}\frac{d}{dt}\int_p \rho(t)\, ds \left[\frac{Q}{P} - \frac{S^2 P}{2R^2 Q}\left(1 + \frac{N^2}{M^2}\right)\right] \qquad (11)$$

This error can be removed by choosing the ratios so as to make the quantity in the second bracket equal to zero. In the 1976 redshift experiment[9] the transponder ratio, N/M, was 221/240. We chose P/Q = 76/49 and R/S = 82/55, so that the resulting error was 2.5×10^{-5} of the ionosphere Doppler shift in the one-way link. We estimated that under typical ionospheric conditions $\Delta f_{DI}/f$ could have been as large as 3×10^{-10}, which is comparable to the relativistic and gravitational effects we measured[10]. Without cancellation of the ionospheric effect the experiment would not have succeeded.

$$f_{DI} = \frac{1}{fc}\frac{d}{dt}\int_p \left(1 - \frac{\rho e^2}{8\pi^2 \varepsilon_o m}\right) ds$$

$$= -\frac{e^2}{8\pi f c \varepsilon_o m}\frac{d}{dt}\int_p \rho(t)\, ds \qquad (10)$$

Here p is the propagation path over which the integral is taken. The integral represents the columnar electron density in the path. When we follow the ionospheric Doppler frequency shifts through the two transponder links and the clock downlink, we find that the ionosphere contributes a frequency error at the output from mixer M3 of Figure 5 in the amount

$$|f_{I\,error}| = \frac{e^2}{8\pi f c \varepsilon_o m}\frac{d}{dt}\int_p \rho(t)\, ds \left[\frac{Q}{P} - \frac{S^2 P}{2R^2 Q}\left(1 + \frac{N^2}{M^2}\right)\right] \qquad (11)$$

This error can be removed by choosing the ratios so as to make the quantity in the second bracket equal to zero. In the 1976 redshift experiment[9] the transponder ratio, N/M, was 221/240. We chose P/Q = 76/49 and R/S = 82/55, so that the resulting error was 2.5×10^{-5} of the ionosphere Doppler shift in the one-way link. We estimated that under typical ionospheric conditions $\Delta f_{DI}/f$ could have been as large as 3×10^{-10}, which is comparable to the relativistic and gravitational effects we measured[10]. Without cancellation of the ionospheric effect the experiment would not have succeeded.

2.2 The 1976 GP-A Gravitational Redshift Experiment

The fractional output frequency variations obtained by subtracting one-half of the two-way Doppler cycles from the one-way cycles received by the earth station is given in the expression:

$$\frac{f_s - f_e}{f_0} = \frac{(\phi_s - \phi_e)}{c^2} - \frac{|\vec{v}_e - \vec{v}_s|^2}{2c^2} - \frac{\vec{r}_{se} \cdot \vec{a}_e}{c^2} \qquad (12)$$

Here the total frequency shift is $f_s - f_e$, and f_0 is the clock downlink frequency. The first term is the gravitational redshift resulting from the difference in the Newtonian gravitational potential, $(\phi_s - \phi_e)$, between the two clocks. The second term is the second-order Doppler effect of special relativity from v_e and v_s which are the velocities of the earth station and the spacecraft. The third term is the result of the acceleration of the earth station during the light time, r/c, owing to the earth's rotation; $\vec{r}_{se}$ is the vector distance between the spacecraft and earth station, and $\vec{a}_e$ is the acceleration of the earth station in an inertial frame. For the 1976 test, an earth-centered frame with axes aimed at the fixed stars was sufficiently "inertial" to satisfy the needs of the experiment.

During the two-hour near-vertical flight, the first-order Doppler shifts were as large as $\pm 2 \times 10^{-5}$ and the noise from ionospheric and tropospheric propagation effects was at a level of about 1×10^{-12} at t ~100 sec, as shown in the top left curve of Figure 2. After the frequency variations predicted in Equation 12 were fitted to the data, we concluded that the error in the fit of the data was within $(+2.5 \pm 70) \times 10^{-6}$ of Einstein's

prediction.[11] The residuals were analyzed after subtracting the predicted frequency variation over the time of the mission and the resulting Allan standard deviation of the frequency residuals is shown in Figure 6. Here we see that the stability of the frequency comparison made through the three-link system over signal paths of 10,000 km, in the presence of Doppler shifts of magnitude ± 44 kHz plus the ionospheric and tropospheric noise shown in Figure 2, is comparable to the frequency comparison made between the two reference masers in the same room, reaching 7×10^{-15} stability at about 10^3 sec.

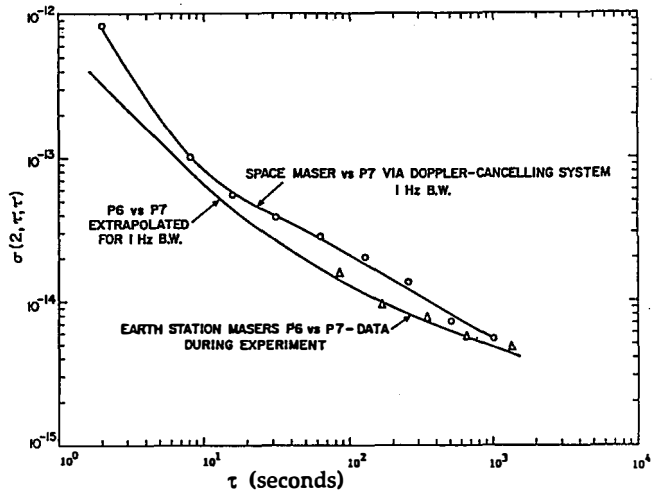

Figure 6 Allan Variance of GP-A Frequency Residuals

2.3 A Symmetrical Four-Link System to Provide Time-Correlated Doppler Data

The three-link system can be made symmetrical by providing a transponded signal back to the spacecraft as shown in Figure 7. Here one-way, two-way, and Doppler-cancelled data are recorded at both stations of the system in terms of the proper time scale kept by the station's clock. In cases where the stations are widely separated, so that the light time between stations is long compared to the intervals required for measurements, a dominant, spatially localized noise process can be cancelled *systematically* by time-correlating the data from the two stations. To illustrate this process, Figure 10 (of section 3.2) shows the continuum of space-time paths of the four signals in Figure 7. Here the dots signify the clocks, and the arrows, $E_1(t)$ and $E_2(t)$, signify signal outputs representing earth-based one-and two-way data at a particular epoch in the continuum. $S_1(t)$ and $S_2(t)$ represent one- and two-way data recorded in space. By time-correlating the Doppler responses we can systematically cancel a strong localized noise source such as the earth's troposphere and ionosphere This technique also offers possibilities for detecting pulsed gravitational radiation.

CONCEPT OF 4 LINK TIME CORRELATED DOPPLER SYSTEM

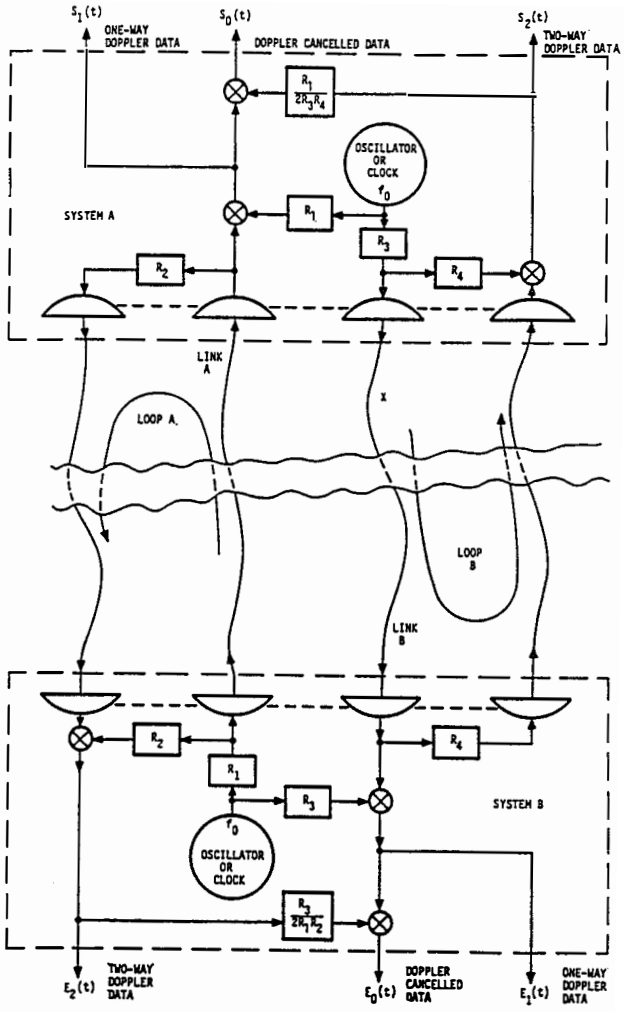

Figure 7. A four-link Doppler cancelling system that allows time correlated data to be obtained both at the earth and space terminal.

The Doppler-cancelled signal outputs $S_o(t)$ and $E_o(t)$ in Figure 7 contain relativistic and gravitational information that can also be time correlated. The counterpart to Equation 12 for effects at the spacecraft, $S_o(t)$, is given in Equation 13.

$$S_o(t) = \frac{\phi_e - \phi_s}{c^2} - \frac{|\vec{v}_e - \vec{v}_s|^2}{2c^2} - \frac{\vec{r}_{es} \cdot \vec{a}_s}{c^2} \qquad (13)$$

By adding the two time-ordered data sets in Equations 13 and 12, we cancel the first term and double the magnitude of the second term representing the second-order shift. Conversely, if we subtract the data sets, we double the first-term representing the gravitational red (blue) shift and cancel the second term. In both instances we must account for the acceleration of the earth and space stations along the line of sight in a suitable inertial frame.

3. Future Tests of Relativistic Gravitation with Clocks

3.1 A PossibleTest with a Clock in a Highly Eccentric Earth Orbit

The original concept for testing the gravitational redshift called for operating a spaceborne clock in a spacecraft placed in a highly eccentric 24-hour earth orbit.[12] Low inclination orbits with eccentricities as high as 0.6 can produce apogee-to-perigee redshifts of about 4.8×10^{-10}, and still keep the spacecraft in view of an earth station with a minimum elevation angle greater than 15 degrees [13]. Accompanying the redshift there is a second-order Doppler shift of comparable magnitude, which produces a combined frequency variation of 9.6×10^{-10} in the Doppler cancelled data described in Equation 12. The Russian Space Agency RADIOASTRON mission, which will operate a spaceborne radiotelescope will be in a highly eccentric orbit and if equipped with an H-maser, could provide a substantially improved test of the gravitational redshift from 70 parts per million test made in 1976, to 2 parts per million.

3.2 A Proposed Extension of the GP-A Experiment to Test General Relativity with a Solar Probe

Studies have been conducted of relativistic gravitation tests with a clock in a space probe in a polar orbit approaching within 4 solar radii of the sun's center.[14] The 14 hour time of travel from pole-to-pole coincides with the interval of the best performance of today's hydrogen masers.

During the 10 hours before and after perihelion, the first-order redshift, Φ_1/c^2, in equation 14, below, varies from 5.3×10^{-7} at perihelion to 2.0×10^{-7} at times ±10 hours from perihelion. During the same interval, the second-order redshift, $2\,[\Phi_1/c^2]^2$, varies from 2.81×10^{-13} to 4×10^{-14}, as shown in Figure 8. Taking the Allan standard deviation of today's H-masers over 10 hours averaging time as 6×10^{-16}, the predicted precision of measurement of the first-order redshift measurement is 1.8×10^{-9}, the corresponding precision for the second-order measurement is 2.5×10^{-3}.

The sun's gravitational potential is complicated by having a number of multipole components. The largest of these is the solar quadrupole moment, $J_{2\odot}$,

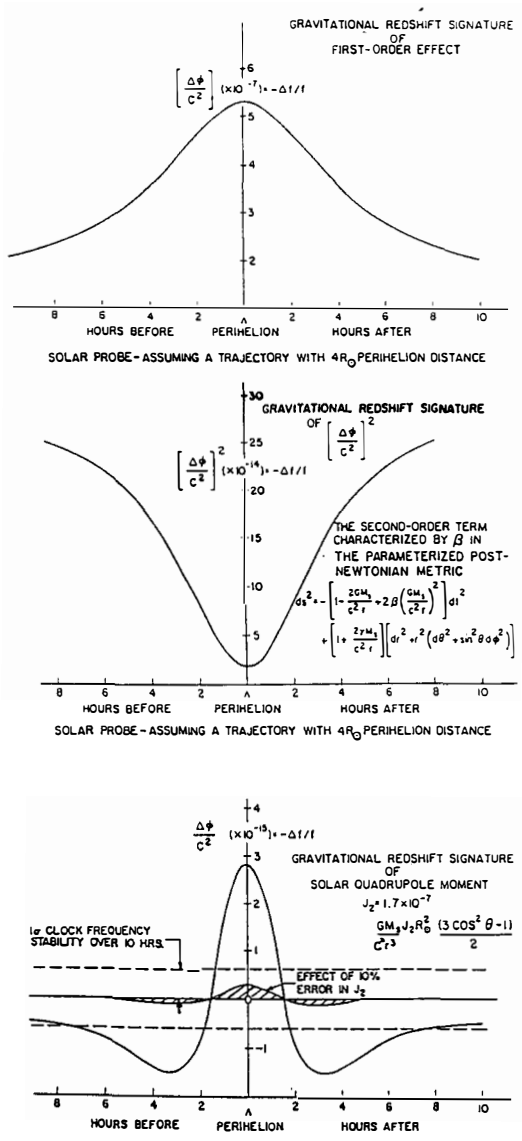

Figure 8 Signatures expected in the Doppler Cancelled Data from the Solar Probe

which must be accounted for in the measurement of the second order term in the redshift. Measurements of J_2 have been made from solar oscillations,[15] and we can estimate the precision in these measurements from the behavior of the J_2 signature in the data during the 14-hour pole-to-pole passage, assuming $J_2 = (1.7 \pm 0.17) \times 10^{-7}$.

At order c^{-2} the first-order redshift has the following behavior:

$$F(\phi, c^2) = \frac{\Phi_1}{c^2} + \frac{\Phi_2}{c^2} = \frac{\mu}{r} + \frac{\mu}{r^3} J_2 R^2_{sun} \frac{3\cos^2\vartheta - 1}{2} \qquad (14)$$

where $\mu = GM_{sun}/c^2$. At perihelion, $r = 4R_{sun}$, $J = \pi/2$, and $\Phi_2/c^2 = -2.8 \times 10^{-15}$. At about ±7 hours from perihelion, J=0, $r = 8R_{sun}$, and $\Phi_2/c^2 = +7.0 \times 10^{-16}$.

The frequency variation caused by the J_2 contribution to the sun's redshift is shown in Figure 8 before and after perihelion. Its peak-to-peak magnitude is 3.5×10^{-15}. If we have an error of 10% in the estimate of J_2, the uncertainty in its contribution to the redshift over this interval is comparable to the instability of the clock.

To achieve the precision of measurement of the second-order redshift and of J_2, the position of the probe must determined to 1m rms. and its velocity to within about 1 mm sec^{-1}.

An important feature that makes this experiment possible is the ability to take Doppler-cancelled data at the probe. Figure 9 shows how the localized noise near earth can be cancelled by correlation. While the spacecraft Doppler cancellation system can systematically remove the effect of the tropo-iono noise when it produces the $S_0(t_i+2R/c)$ data, this is not the case for the earth station Doppler-cancelled output E_0. In the earth station cancelled Doppler there would be about 1000 sec of time delay between the uplink transmission and reception from the transponder. During this interval the combined atmospheric and ionospheric delay could have varied considerably.

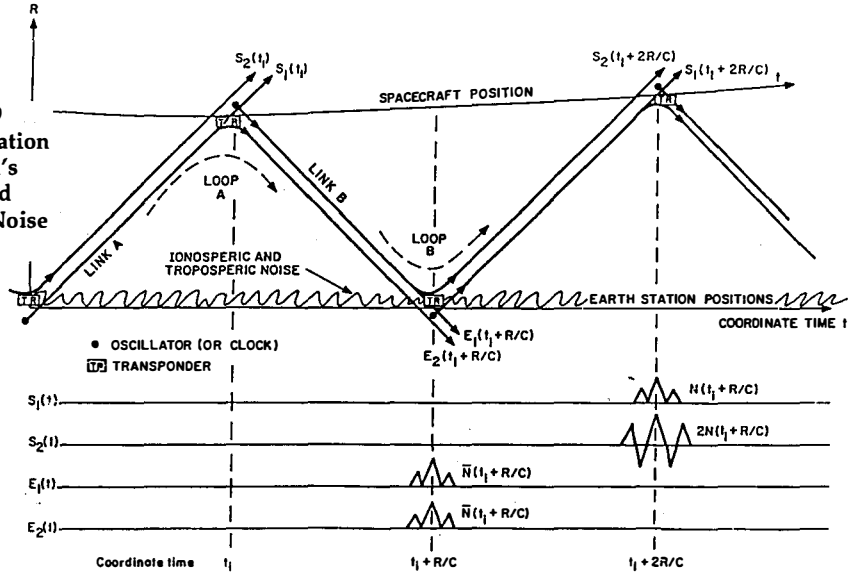

Figure 9 Cancellation of Earth's Iono and Tropo Noise

3.3 Detection of Pulsed Gravitational Radiation using Doppler Techniques

Long term deep,space missions such as the Solar Probe provide opportunities to search for gravitational radiation using Doppler techniques.[16),17),18)] A signal transmitted by a highly stable microwave (or laser) transmitter and detected by a receiver located at a distance that is greater than about one-half the wavelength of the gravitational wave will exhibit a freqency shift. An example of detection[19)] of a pulsed gravitational wave using the four-link measurement system is shown in Figure 10. Here the wavefront of the gravitational pulse is assumed to intercept the earth-probe line at an angle, θ = 60 degrees. The effect of this pulse would be observed three times in the Earth 2-way Doppler trace as follows:

$$\frac{df}{f} = \frac{(1-\mu)\psi(t_R)}{2} - \mu\psi\left[t_R - L\frac{(1+\mu)}{c}\right] + (1+\mu)\psi\left(t_R - 2\frac{L}{c}\right) \qquad (15)$$

- by a Doppler shift of the gravitational wave disturbing the earth station at $t=t_1$, while it is receiving a signal transmitted earlier by the spacecraft.
- by its echo when the earth station receives a transponded signal at $t = t_1 + 2R/c$.
- by the disturbance when the gravitational wave arrives at the spacecraft at time t_2 and is later reported at earth at $t = t_2 + R/c$.

The one-way transmission from the spacecraft would show the pulses at t_1 and at $t_2 + R/c$. The spacing of the pulses, the magnitude and sign of their time signature, $\psi(t)$, and the relative magnitude and sign of the signature are described by a single parameter, $\mu = \cos\theta$ [20),21)]. Here t_R signifies arrival time at the first station. A similar set of five observations of the same gravitational pulse is available at the spacecraft. In this case $\mu = \cos(\pi+\theta)$.

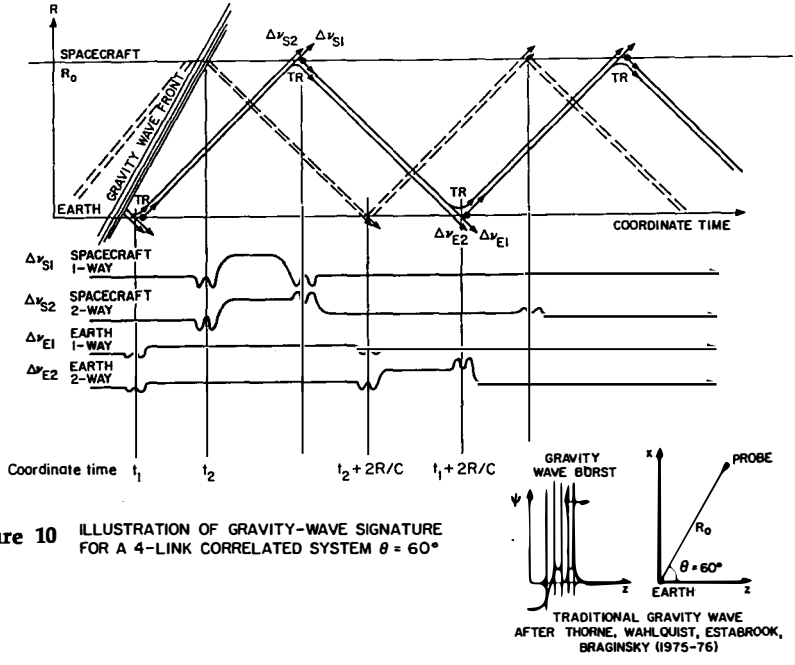

Figure 10 ILLUSTRATION OF GRAVITY-WAVE SIGNATURE FOR A 4-LINK CORRELATED SYSTEM $\theta = 60°$

For earth based operation, tropospheric noise will substantially degrade the stability of a signal. Studies show that the Allan deviation of the tropospheric noise for signals passing vertically has a $t^{-2.5}$ behavior for intervals between 20 and 200 sec, with σ_y (100 sec) = 8×10^{-14}, as shown in Figure 2[22]. By implementing the process shown in Figure 8, it is possible to account for spatially localized sources such as near-earth tropospheric and ionospheric variations and earth station antenna motion. By operating at microwave frequencies at K band or higher, noise from the solar corona ionization will be reduced and the principal non-gravitational noise sources will likely be from the buffeting of the space vehicles by light pressure, particle collisions, and sporadic outgassing of the spacecraft. Since these disturbances are localized at the ends of the system, the time signatures of the noises can be distinguished from the patterns expected from pulsed gravitational waves, which have signatures that depend only on the parameter μ of Equation 15.

4. High Resolution Very Long Baseline Interferometry (VLBI) Astronomy in Space

4.1 The Effect of Oscillator Instability on the Measurement of Angles

The highest present levels of angular resolution of any astronomical technique are now made with Very Long Baseline Interferometry (VLBI) techniques shown in Figure 11.[23] Here, two radio telescopes, separated by a distance, L, each detect the arrival of radio noise signals from a distant radio star. After heterodyning to a lower frequency, the noise signals are recorded as a function of time and the two sets of noise data are time-correlated. The observable quantities from the correlation process are the correlated amplitude and the relative phase of the signals. VLBI measurements have been used in light deflection tests of relativistic gravitation.[24]

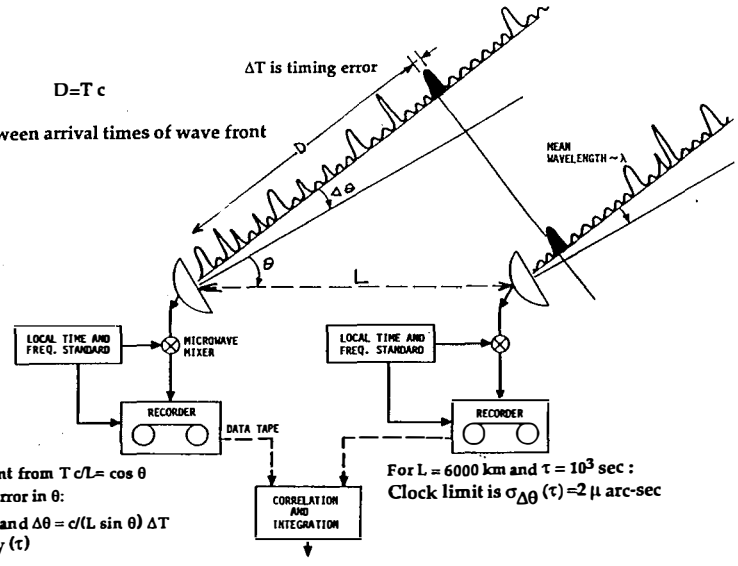

Figure 11
Very Long Baseline Interferometry

The stability limit on the successive measurements of angle imposed by the oscillator instability on successive measurements of angle taken t seconds apart is

$$\sigma_{\Delta\theta}(\tau) \sim \frac{c\,\tau\,\sigma_y(\tau)}{L \sin\theta}, \tag{16}$$

where θ is the angle between the propagation vector and the baseline. The result of correlating the noise data obtained from a common source by the two stations is to produce fringes. The spacing between fringes is $\lambda/L\ \mathrm{Sin}\theta$, where λ is the average wavelength of the signals arriving at the antennas. The visibility of the fringes depends on the extent to which the signals arriving at the antennas are correlated.

The angular resolution of the interferometer is given by the change of fringe phase, ϕ, with θ

$$\frac{d\phi}{d\theta} = \frac{2\pi L}{\lambda} \tag{17}$$

The error in successive angular measurements owing to the instability of the clocks in a terrestrial system with L = 6000 km, assuming $\sigma_y(10^3\ \mathrm{sec}) = 1 \times 10^{-15}$, and $\theta = \pi/2$, is given by

$$\sigma_{\Delta\theta}(10^3\ \mathrm{sec}) = 5 \times 10^{-11}\ \mathrm{rad\ or}\ 2\ \mu\ \mathrm{arcsec}.$$

However this is far smaller than the present actual limit of 100 μ arcsec level from terrestrial stations operating at 7 mm wavelength.[25] because the limitations imposed by tropospheric and ionospheric fluctuations are far more serious than clock instability.

By operating VLBI stations in space, limits in angular resolution owing to tropospheric and ionospheric propagation and terrestrial baseline distances can be overcome . A successful demonstration of a spaceborne radio telescope operating as a VLBI terminal was made in 1986 [26] using NASA's orbital Tracking and Data Relay Satellite System system as a spaceborne radio telescope in conjunction with a number of radio telescopes on earth.

To estimate the limits that a spaceborne two station system could achieve, consider a system where $L = 5 \times 10^6$ km, $\sigma_y(10^4\ \mathrm{sec}) = 4 \times 10^{-16}$, and $\theta = \pi/2$. In this case,

$$\sigma_{\Delta\theta}(10^4) = 2 \times 10^{-13}\ \mathrm{rad\ or}\ 0.05\ \mu\mathrm{arcsec}.$$

For $\lambda = 1$ mm we have $\lambda/L = 2 \times 10^{-13}$ rad and we see that the limit imposed by clock stability (with 10^4 sec integration time) will allow resolution of fringes at 1-mm wavelengths in a spaceborne system with baseline distances of 5×10^6 km. While *relative* positions of radio stars, and features of their brightness distribution, can be made with a precision of a few tenths of a milliarcsecond, the *absolute* directions in space of the baselines between VLBI stations will depend on the choice of a frame of reference. For terrestrial measurements, this reference is usually obtained from separately determined VLBI determinations that orient the polar axis and rotation of Earth with reference to the positions of very distant radio sources.

4.2 *A Spaceborne Four Terminal (VLBI) Array that Establishes an Inertial Reference Frame, based on the Velocity of Light and the Sagnac Effect*

Defining the orientation of a spaceborne VLBI system poses an interesting problem. Distant radio stars define the conventionally used inertial frame, however, by invoking the Sagnac effect,[27] we can define another inertial frame based on the velocity of light.

Figure 12 shows an array of four space borne VLBI stations in the form of a tetrahedron with baseline distances of 5 million kilometers that defines a three-dimensional figure in space. (The station separations need not be equal.) Each station contains a clock that is synchronized to a coordinate time scale and is connected to its three neighbors by the four link system shown in Figure 7.[28] The six baseline distances can be precisely measured using techniques discussed earlier so that the *configuration* of the array can be precisely described as a function of a coordinate time scale defined by the atomic clocks.

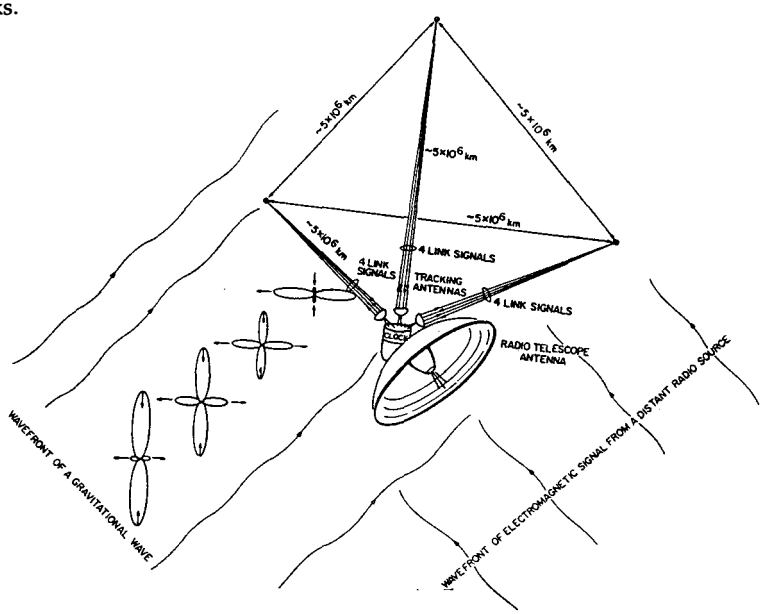

Figure 12 A Tetrahedral Array of Spaceborne Radiotelescopes

From the Sagnac effect we have that the difference in time of arrival of light signals sent in opposite senses about a closed path on a surface rotating at Ω rad/second with area, A, projected perpendicular to the axis of rotation is

$$\Delta\tau = 4\Omega A/c^2 \qquad (18)$$

By measuring the difference in arrival times of signals going in opposite senses about a triangle defining one face of the tetrahedron, we can obtain the component of rotation normal to that face. From the four triangles that define the tetrahedron we have an over determination of the rotation and can make an estimate of the accuracy of its measurement.

For the array shown in Figure 12, the limitation of the detection of changes in rotation rate, $\Delta\Omega$, is 1.2×10^{-15} rad/sec. If the array is located at 1 AU from the sun, such a rotation measurement would include the Einstein–deSitter precession of 2×10^{-2} arc-sec/yr (3×10^{-15} rad/sec) owing to the bending of space-time by the sun's gravity.

This array offers possibilities for astrometric observations as well as for imaging radio sources. While the proper motions of these radio sources could be measured relative to each other and provide a traditional inertial frame, they could also be referenced to the local inertial frame defined by the velocity of light. Because the system could compare the frame of reference defined by the most distant radio sources with a different inertial frame defined locally by the velocity of light, this comparison opens, in a modern context, the questions on inertial frames raised long ago by Bishop Berkeley, and more recently by Ernst Mach and others. Could this system reveal new aspects of the behavior of the missing matter in the universe?

5. Conclusions

Progress in experimental tests of relativistic gravitation has been agonizingly slow even though technology for making precision measurements is evolving ever more rapidly. Since the mid 1950's the stability of atomic clocks (or oscillators) has been improving by a factor of about 10 every decade. Atomic clocks, lasers, millimeter wave devices, microelectronics, and photo-electronics devices are also rapidly improving in performance. It is certain that these new technologies will lead us to new concepts for experiments from which we will learn more about our universe.

6. References and Bibliography

[1] J. Ruttman and F.L. Walls, Proc. IEEE, vol. 79, 1991.

[2] A.J. Berlinsky and W.A. Hardy, In proc 13th Annual Precise Time and Time Interval Conference, NASA Conference Publication No. 2220, 1982, p.547.

[3] R.F.C. Vessot, M.W..Levine, and E.M..Mattison, in *Proc. of The Ninth Annual Precise Time and Time Interval (PTTI) Meeting*, NASA Goddard Space Flight Center Nov 29-Dec 1; pp 549-570.

[4] R. F. C. Vessot, E. M. Mattison, R.L. Walsworth, Jr., I. F. Silvera, H. P. Godfried, and C. C. Agosta, *IEEE Trans. on Instrumentation and Measurement* IM-36 No. 2, 588 (1987).

[5] R.F.C.Vessot, E.M. Mattison, W.J. Klepczynski, G.M.R. Winkler, I.F. Silvera, H.P. Godfried, and R.L. Walsworth, in *Proc. Fourth Marcel Grossman Meeting on General Relativity* (R. Ruffini, Ed.) Rome, Italy, June 17-21, 1985

[6] D. J. Wineland, J.C. Bergquist, J.J. Bollinger, W.M. Itano, D.J. Heinzen, S. L. Gilbert, C.H. Manney, and M.G. Raizen, *IEEE Trans. on Ultrasonics, Ferroelectrics and Frequency Control*, vol. 37, no. 6, Nov. 1990.

[7] L.A. Rawley, J.H. Taylor, M.M. Davis, and D.W. Allan, *Science*, vol. 238.

[8] A.J.Tucker and B.M. Fannin *Journal of Geophysical Research, Space Physics*, 73, No. 13, 4325 (1968)

[9] R.F.C. Vessot and M.W. Levine, in *Proc. Twenty-eighth Annual.Symp. Frequency Control*, U.S. Army Electronics Command, Ft. Monmouth, NJ, 1974, pp. 408-414.

[10] R.F.C. Vessot and M.W. Levine, NASA Redshift Experiment Final Redshift Report, GPA Project Report, Contract NAS8-27969.

[11] R.F.C. Vessot, M.W. Levine, E.M. Mattison, E.L. Blomberg, T. E. Hoffmann, G.U. Nystrom, B.F. Farrell, R. Decher, P.B. Eby, C.R. Baugher, J.W. Watts, D.L. Teuber, and F.D. Wills, *Phys. Rev. Lett.*, vol. 45, pp. 2081-2084, Dec. 1980.

[12]D. Kleppner, R.F.C. Vessot, and N.F. Ramsey, *Astrophys. Space Sci.* , vol. 6, pp. 13-32, 1970.
[13]L.L. Smarr. R.F.C. Vessot, C.A. Lundquist, R. Decher, and T. Piran, *Gen. Rel. and Grav.* vol. 15, no. 2, pp. 129-163, 1983.
[14] M. Neugebauer and R.W. Davies, *A Closeup of the Sun*, JPL Publications 78-70, NASA, 1978.
[15] T. M. Brown, J. Christensen-Dalsgaar, W.A. Dziembowski, R. Goode, D.O. Gough, and C.A. Morrow, *Astrophys. J.*, vol. 343, p. 526, 1989.
[16] T. Piran, E. Reiter, W.G. Unruh, and R.F.C. Vessot, *Phys. Rev. Lett., D*, 34, no. 4, p. 984, 1986.
[17] F. B. Estabrook, *ACTA Astronautica*, vol. 17, no. 5, pp. 585-587, 1988.
[18]J. W. Armstrong, J.D. Anderson, and E.L. Lau, in *Proc. of Twenty-first Annual Precise Time and Time Interval (PTTI) Applications and Planning Meeting*, Redondo Beach, CA. Nov. 28-30, 1989, pp. 259-263.
[19] A. J. Anderson, *Nature*, vol. 229, pp. 547-548, 1971.
[20] F. B. Estabrook and H.D. Wahlquist, *Gen. Rel. Grav.*, vol. 6, pp. 439-447, 1975.
[21] K. S. Thorne and V.B. Braginsky, *Astrophys. J. Lett.*, vol. 204, L1, 1976.
[22]A.E.E. Rogers, A.T. Moffet, D.C. Backer, and J.M. Moran, *Radio Sci.*, vol. 19, no. 6, pp, 1552-1560, 1984.
[23]A.E.E. Rogers and J.M. Moran, Chapter 5, "Interferometers and Arrays," Chapter 5 in *Methods of Experimental Physics*, Astrophysics, M.L. Meeks, Ed., vol. 12. New York: Academic Press, 1976.
[24]E. B. Formalont and R.A. Sramek, *Phys. Rev. Lett.*, vol. 36, p. 1475, 1976.
[25] N. Bartel, et al., *Nature*, vol. 334, no. 6178, pp. 131-135, 1988.
[26] G.S. Levy, et al. *Acta Astron.*, vol. 15, no. 6/7, pp. 481-487, 1986.
[27] E.J. Post, "Sagnac Effect," *Rev. Mod. Phys.* , vol. 39, p. 475, 1967.
[28] R.F.C. Vessot, in *Advances in Space Research*, Pergammon Press, vol.9, No. 9, 1989.